Karlsruher Institut für Technologie

FAKULTÄT FÜR PHYSIK

PHYSIKALISCHES PRAKTIKUM FÜR FORTGESCHRITTENE

PRAKTIKUM MODERNE PHYSIK

Gruppe Nr. _____ Kurs: **Mo1** **Mo2** **Mi3**

zutreffendes bitte ankreuzen

aktuelles Semester angeben

Versuch: _____

Namen: _____

_____

Assistent: _____

durchgeführt am: _____

Protokollabgabe am: _____

_____

vom Betreuer auszufüllen

Note gesamt [+] [0] [-]

Anerkannt: _____

(Datum Unterschrift)

Datum Rückgabe: _____

Bemerkung:

Contents

List of Figures

1. Introduction

The quantum Hall effect (QHE) was discovered in 1980 and is subject to the unexpected behavior of the classical Hall effect in the regime of strong magnetic fields. It is now used to provide a resistance standard based on natural units, refining the SI system. This experimental report investigates the QHE using a semiconductor heterostructure sample, describing the obtained data and using the results to calculate the fine structure constant. After introducing the theory of classical and quantum Hall effect, as well as two-dimensional electron gases, chapter two describes the experimental setup and measurement procedure. The obtained data is then analyzed in chapter 3.

1.1 Classical Hall Effect

The classical Hall effect, discovered by Edwin Hall in 1879, occurs when a current running through a thin conductor is subject to a magnetic field perpendicular to it. The hereby caused Lorentz force results in the separation of charged particles within the conductor, thus establishing an electric potential between the outer edges of the conductor. The measurable voltage is called the Hall voltage

$$V_H = \frac{B_z \cdot I_x}{n \cdot e \cdot d}, \tag{1.1}$$

Where n equals the density of charges and d the thickness of the conductor. A schematic of the classical Hall effect can be seen in figure 1.1.

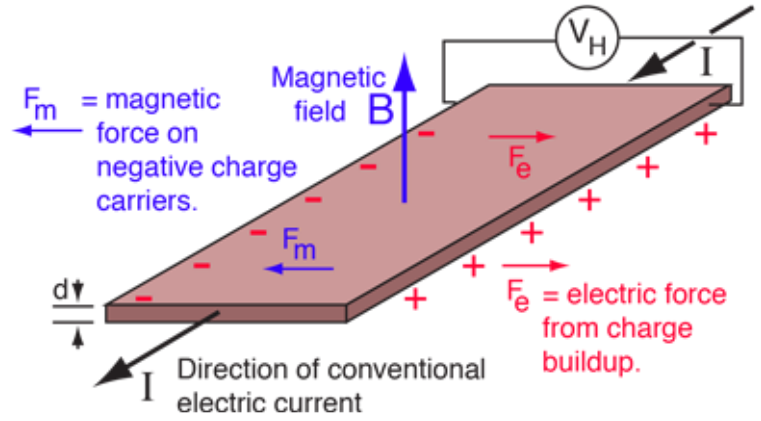

Figure 1.1: Schematic of the classical Hall effect. Showing acting magnetic forces in blue, electric forces in red, and flowing current and Hall voltage in black. From [2]

Due to the additional Hall voltage two resistances can be measured. The longitudinal resistance in the direction of the current and the transversal Hall resistance, emerging from the Hall voltage. The total resistivity can therefore be written as a matrix

$$\begin{pmatrix} E_x \\ E_y \end{pmatrix} = \begin{pmatrix} \rho_{xx} & \rho_{xy} \\ -\rho_{xy} & \rho_{yy} \end{pmatrix} \begin{pmatrix} J_x \\ J_y \end{pmatrix}. \tag{1.2}$$

Since the longitudinal resistivity is unchanged by the perpendicular magnetic field, the Hall resistivity is computed from equation 1.1

$$R_H = \frac{V_H}{I_x} = \frac{B_z}{n \cdot e \cdot d}. \tag{1.3}$$

Thus the classical interpretation of the Hall effect expects the Hall resistivity to be proportional to the magnetic field strength.

1.2 Two-Dimensional Electron Gas

The two-dimensional electron gas (2DEG) is a model concept in solid-state physics. It is achieved by confining the degrees of freedom from a three dimensional electron gas to two dimensions. This confinement causes the energy for motion in the confined direction to be quantized in discrete energy levels. A 2DEG can be realized within a pn-junction, where p- and n-doped semiconducting material is arranged side by side in a single semiconductor. When the depletion layer forms it is confined along the axis where the p- and n-doped material is aligned and thus acts as a 2DEG.

1.3 Quantum Hall Effect

The energy distribution of a 2DEG can be further quantized by applying a large magnetic field. By reducing the dimensionality an increase in Coulomb interactions causes correlated states, leading to the fractional QHE. When observing the classical hall effect, the electrons are confined to the edge of the sample. With increasing magnetic field strength, the energy levels are then quantized into Landau levels. The current flowing at the edges of the conductor leads to specific edge states that are topologically protected, causing a quantized Hall conductance. Experimentally the Hall voltage is observed to show plateaus at certain magnetic field strengths instead of behaving linear, like the classical Hall effect predicts. Those plateaus are a direct result of the quantization of energy distribution. They are formed whenever a Landau level is fully occupied, because enough electrons have to accumulate in order to pass the band gap to the fill the next one.

This quantum mechanical interpretation introduces the flux quantum ($\frac{h \cdot c}{e} = \Phi_0$) and the dimensionless variable

$$\nu = \frac{n \cdot \Phi_0}{B}, \tag{1.4}$$

which represents the electron density n over the density of flux quanta $\frac{B}{\Phi_0}$. The Hall resistivity,

$$\rho_{xy} = \frac{h}{e^2 \cdot \nu}, \tag{1.5}$$

then shows an inverse proportionality with respect to ν.

In experimental observations the value of the Hall resistivity at each step shows to be a multiple of $\frac{h}{e^2}$ as expected from equation 1.5. Here, the longitudinal resistivity fluctuates alongside the Hall resistivity, notably it is observed to be close to zero whenever the Hall resistivity reaches a plateau. Therefore causing no heating while the system is in a quantum Hall state. The QHE is separated in the fractional and integer QHE, referring to fractional or integer values of ν.

1.3.1 Requirements for Samples to Show the Quantum Hall Effect

To optimize the measurement of the QHE samples used should be two dimensional electron systems, like 2DEGs. They have to provide high mobility and purity, as well as well-defined edges. This way scattering events can be lowered, whilst well-defined Landau levels and edge states are ensured. Those qualities have to be present at the low temperatures of the experiment, used to prevent thermal fluctuations and obtain a a less smeared Fermi distribution.

1.3.2 Impacts of Temperature and Current Changes on the QHE

Higher temperatures cause inaccuracies mostly through thermal excitations, causing electrons to jump between states and therefore smeared Landau levels. As a result the transition regions between plateaus increase, since it requires more energy to fill the smeared Landau levels. Similarly correlated states become more fragile and are increasingly suppressed.

By increasing the sample current, the increase in electric field strength can cause more scattering events and even a breakdown of quantization if electrons are enabled to jump between Landau levels. These effects are not expected to increase linear with the current and can also lead to temperature effects mentioned above through heating.

1.3.3 Zeeman Splitting and Coupled States in the QHE

This experiment observes the integer QHE, since the magnetic field strength required to observe the fractional QHE can't be reached with its setup. The fractional QHE is caused by correlated states and the spin-split Landau levels, a degeneracy of Landau levels associated with spin, caused by Zeeman splitting. These degeneracies cause fractional values of ν, referring to closely separate Landau levels.

1.3.4 Fine Structure Constant

Since the quantum Hall plateaus are located at multiples of $\frac{h}{e^2}$, an analysis of experimental data can provide a value for this reoccurring constant. The fine structure constant

$$\alpha = \frac{e^2}{4\pi\epsilon_0\hbar c} \approx \frac{1}{137} \tag{1.6}$$

can then be calculated using the experimental data from the quantum Hall plateaus.

2. Experiment

This chapter handles the detailed experimental procedures and setup utilized to observe the QHE (QHE) at low temperatures. The setup employs a cryostat and precise control of magnetic fields to study the properties of a two-dimensional electron gas (2DEG) in semiconductor heterostructures. This experimental investigation not only enables a deeper understanding of fundamental quantum mechanics but also allows for the exploration of state-of-the-art topics in low-temperature physics.

2.1 Experimental Setup

The cryostat used in this experiment, that is depicted in the Figure 2.1 is a ^{4}He cryostat capable of achieving temperatures as low as 2 K. Initial cooling of the He tank is executed with liquid nitrogen (l-N_2, $T_S = 77$ K), subsequently expelled by compressed air before the introduction of liquid He. The He-dewar is insulated by a vacuum and super-insulation foil to minimize thermal exchange.

2.1.1 Cryostat Description

The heart of the experimental setup is the cryostat, designed for low-temperature operations:

- The **sample chamber** is a double-walled tube maintained under vacuum to thermally isolate the sample from the ambient environment and the liquid helium bath.
- Thermal contact to the sample is regulated through a **capillary**, enabling helium gas flow from the bath into the chamber.
- A **resistor** near the sample platform acts as a thermometer, gauging the precise temperatures at which the QHE is observed.

2.1.2 Measurement Setup

The electronic measurements are conducted through a setup, schematically represented in Figure 2.2:

- A DC current source dictates the current I_P through the sample, with voltages U_{xx} and U_{xy} monitored through a voltmeter.
- A switch box enables the selection of voltage contacts, integral to the Hall resistance measurements.
- The temperature-sensitive carbon resistor thermometer circuit, as illustrated, offers acute temperature readings crucial for QHE observations.

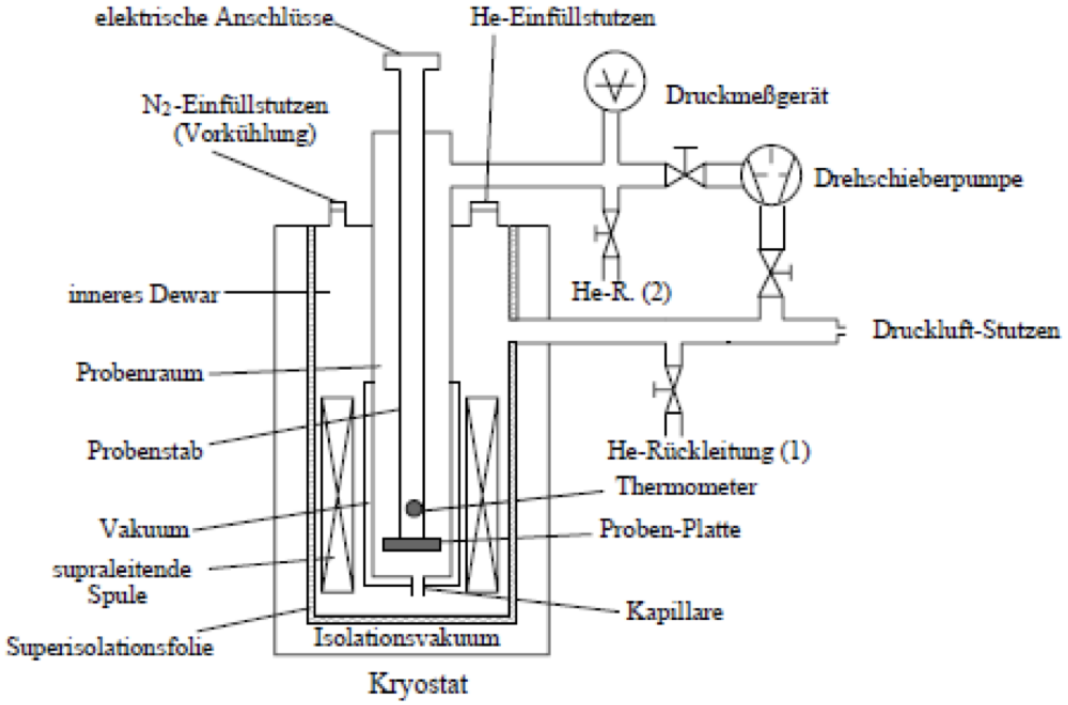

Figure 2.1: Schematic of the experimental set-up

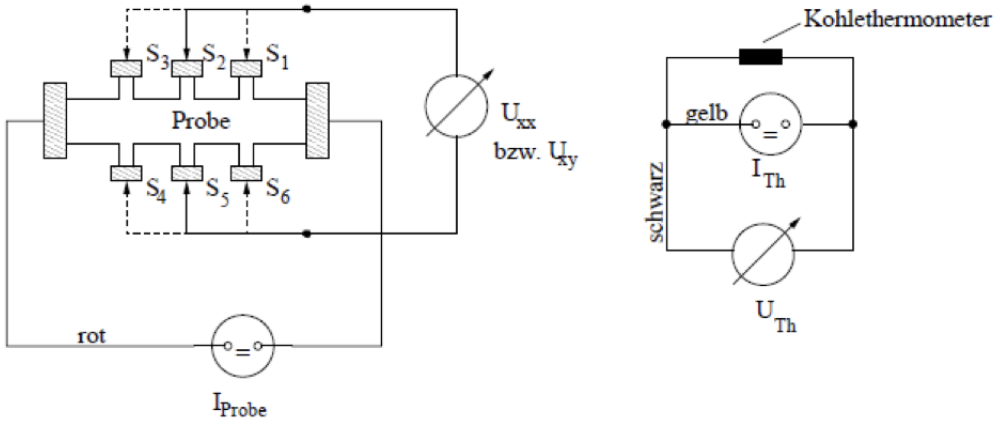

Figure 2.2: Circuit diagrams

2.1.3 Magnet Coil Control

The superconducting magnet is meticulously controlled to ensure precision in magnetic field application:

- The **Set Point** and **Set Rate** functions manage the strength and variation speed of the magnetic field.
- A **Switch Heater** is employed to transition the coil between superconducting and resistive states.
- To modify the magnetic field, the **Sweep** function is used, with the option to hold or zero the field as required.

2.2 The Sample

The cornerstone of the QHE experiment is the two-dimensional electron system, realized in semiconductor heterostructures:

2.2.1 Silicon MOSFET

- The Si MOSFET comprises a p-doped silicon base with a metallic layer on top, permitting gate voltage control over electron density.
- At high gate voltages, an inversion layer forms, trapping electrons in a potential well, thereby realizing the 2DEG.

2.2.2 GaAs-AlxGa1-xAs Heterostructure

- Molecular-beam epitaxy (MBE) is employed to create a near-atomically smooth interface between GaAs and AlxGa1-xAs.
- The presence of a two-dimensional electron gas (2DEG) at the boundary layer facilitates high electron mobility and long mean free paths—characteristics essential for observing clear QHE signals.

2.3 Experimental Procedure

2.3.1 Cooling Down the Cryostat

The initial phase of the experiment required ensuring the accurate placement of the sample within the holder. A verification process was conducted by passing a current of 40 µA—contrary to the standard 50 µA—through the sample and scrutinizing each contact by examining all possible combinations of voltage measurement settings. It's noteworthy to mention that the current was momentarily interrupted as the contacts were switched. This preliminary check, demonstrated by the supervisor, confirmed the functionality of the requisite contacts for the experiment. For subsequent measurements, only two pairs of channels were utilized: channels 1 and 5 to ascertain longitudinal voltage and channels 2 and 5 for transverse voltage readings.

The cryostat's dewar was then evacuated to reach a pressure slightly shy of the intended -1 bar, stabilizing around -0.9 bar against atmospheric pressure due to the system's constraints. After sealing the pump valve and allowing helium gas to enter from the recovery line, the pressure was normalized before a second evacuation. The dewar was left under these vacuum conditions to ensure a pristine environment.

Simultaneously, the sample chamber underwent a dual-cycle evacuation and flooding with helium gas to purge any contaminants. After the second helium flood, the chamber was sealed, and the pressure monitoring equipment was disengaged.

Subsequently, liquid nitrogen was introduced into the cryostat to initiate the cooling process. The cryostat was pre-flooded with helium gas, followed by the meticulous insertion of the nitrogen fill tube, ensuring it was approximately 1.0 cm from the dewar's bottom. Liquid nitrogen was then carefully poured to reach an approximate depth of 55 cm, a level confirmed by a makeshift ruler rather than the conventional level rod. Throughout this process, safety precautions were observed, including the use of protective gloves. Once the cryostat was adequately filled, the nitrogen was allowed to evaporate through a designated hose, and the cryostat cooled down to liquid nitrogen temperature in about 1.5 hours, faster than the anticipated 2 hours.

Following the cooling, the removal of liquid nitrogen from the cryostat was accomplished with meticulous control over the pressure to prevent exceeding a 0.1 bar overpressure. After the complete withdrawal of nitrogen, the cryostat was prepared for the next step by ensuring all helium recovery lines were sealed, and the dewar was again evacuated to the reachable vacuum of -0.9 bar.

This methodical preparation of the cryostat was crucial for achieving the conditions necessary to observe the QHE at the low temperatures required for the experiment.

After meticulously bringing the sample chamber to an approximate pressure of $3 \cdot 10^{-}2$ mbar due to system limitations, the dewar was inundated with helium gas. This process normalized the pressure within the sample chamber, ensuring no blockage by ice in the capillary linking it to the dewar. Following the evacuation of the dewar, a repeat performance of the earlier purging was executed, not just once but twice, to affirm the purity of the environment within.

The next stage involved a ballet of connections and carefully moderated pressures. The helium siphon was introduced to the cryostat and helium canister, establishing a conduit through which liquid helium would flow. The pressure, meticulously kept below 0.1 bar of overpressure, was modulated with a red rubber ball, a rather analog yet precise tool in this high-tech setup. As the helium's surface touched the capillary, the sample chamber's pressure saw a natural increase, signaling the right moment to cease pumping and monitoring. The helium was then filled to a height of about 55 cm, with the level judiciously checked using a rod through the nitrogen nozzle. The rod's oscillations at different points in the helium provided a precise indication of the level, a task performed with the utmost care and, invariably, with cold protection gloves.

Attention then shifted to the resistances within the system: the coil, now bathed in helium, registered a resistance of zero Ohms, indicating the onset of superconductivity. Meanwhile, the temperature within the sample chamber was gauged by introducing a minimal current through a resistor and consulting the R(T) calibration chart. The observed resistance of 2317 Ohm corresponded to a temperature of 4.4 K, slightly above the boiling point of helium. This delicate measurement was a critical step in ensuring that the thermometer did not introduce a heat variable into the system.

With the setup now fine-tuned, measurements as outlined in the subsequent section 2.4.2 could commence. It was imperative that the helium recovery line remained open during these operations, and helium levels were monitored consistently. Should the helium level drop below the critical 25 cm threshold, the superconducting state of the coil would be compromised, rendering any further measurements ineffective.

This precise and controlled environment was the bedrock upon which the observations of the quantum mechanical properties of the system were predicated. The preparation described here provided the necessary conditions for an exploration into the depths of low-temperature physics and the QHE.

2.3.2 Measurements

This section documents the observations obtained from a set of experiments designed to probe the electrical properties of a two-dimensional electron gas under varying magnetic fields and temperatures. The section delineates the empirical findings ascertained from measuring the transverse (Hall) and longitudinal voltages across the sample.

The procedure commenced without altering the temperature of the sample chamber, which was retained at a stable 4.4 K, conducive to the precise requirements of the experiment. At this juncture, voltages U_{xx} and U_{xy} were gauged, consistent with the initial settings, thereby

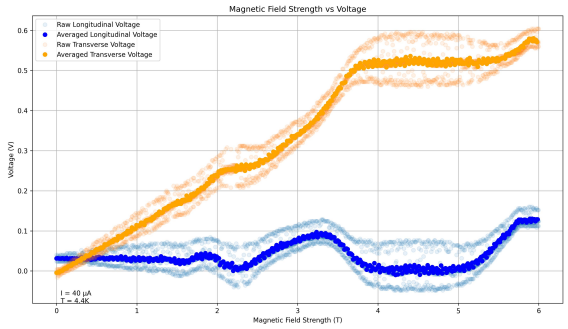

(a) Voltage plot for a current of 40µA at 4.4K.

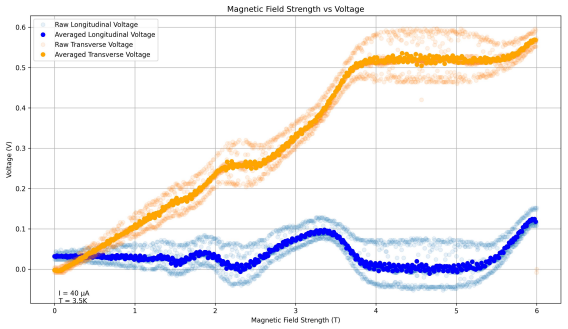

(b) Voltage plot for a current of 40µA at 3.4K.

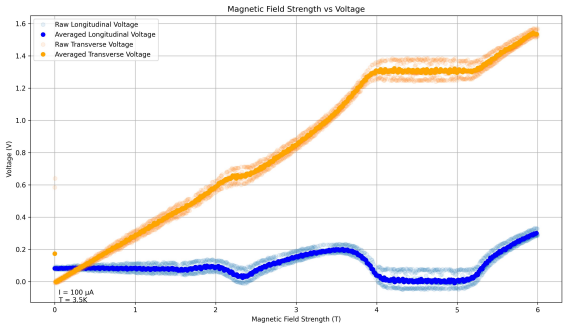

(c) Voltage plot for a current of 100µA at 3.4K.

Figure 2.6: Voltage plots against the magnetic field. (a) Exhibits the behavior at 40µA and 4.4K, (b) demonstrates the response at 40µA and 3.4K, and (c) displays the results at an elevated current of 100µA at 3.4K.

ensuring the validity of comparative analyses. U_{xx}, the longitudinal voltage, was indicative of the potential along the current's direction, while U_{xy} represented the transverse voltage, perpendicular to the current, commonly known as the Hall voltage.

The oscilloscope, diligently configured beforehand to anticipate voltage readings across the magnetic field range of 0 to 6 Tesla, served as the primary instrument for recording these voltages. The sensitivity of the oscilloscope was set with the foresight that the output, especially at peak magnetic field strength and at a current of either 40 µA or 100 µA, would not exceed a few volts, thereby precluding any saturation of the readings.

The longitudinal voltage U_{xx} was captured at a sample current I_P of 40 µA. The magnetic field was incrementally increased from zero to a maximum of 6.0 Tesla, at a rate of 0.5 T/min. The longitudinal voltage, representative of the potential across the entire length of the sample, was recorded both on a voltmeter and concurrently on the oscilloscope.

Simultaneously, the Hall voltage U_{xy} was ascertained at the point where the magnetic field was nullified. The empirical data collected at 4.4 K were complemented with additional readings after the sample was further cooled to 3.4 K, maintaining the same current of 40 µA. These measurements offered insights into the thermal dependency of the Hall and longitudinal voltages.

The investigative scope was broadened by adjusting the sample current to 100 µA while keeping the temperature constant at 3.4 K. The results from this adjustment provided a richer dataset to analyze the interplay between current magnitude and the voltages developed in the presence of a strong magnetic field.

Upon the conclusion of these measurements, the pumping system associated with the sample chamber was deactivated. During the course of the experiment, notable voltages

and the corresponding magnetic field strengths were meticulously catalogued. These data points would serve as critical references for the ensuing analysis.

Incorporated within this section are plots illustrating the transverse and longitudinal voltages as functions of the applied magnetic field, for currents of 40 µA at 4.4 K, 40 µA at 3.4 K, and 100 µA at 3.4 K. These graphical representations (see Figure 2.3) are critical for visualizing the electrical behavior of the system under study and form the bedrock for the analytical discourse to follow in the succeeding chapter.

3. Evaluation/Data Analysis

In this chapter, a careful analysis of the experimental data is presented, with a particular focus on the QHE phenomena observed within a semiconductor sample under varying magnetic field strengths. This analysis is critical for revealing the sample's intrinsic properties, such as charge carrier concentration, and for calculating fundamental constants like the fine structure constant.

The analysis is initiated with an evaluation of recorded curves to pinpoint critical features that exemplify the quantum mechanical behavior of the sample. The first task involves the determination of the longitudinal voltages at the magnetic field strength versus voltage curve extrema. At these points, the curve exhibits local maxima and minima, corresponding to transitions between quantum Hall plateaus. Concurrently, the magnetic field strengths at these points are quantified to delineate the conditions conducive to the manifestation of quantum behavior in the sample.

Attention is then directed towards the Hall voltages, with an aim to calculate the values corresponding to the 'Hall plateaus' identified in the curve. These plateaus are characteristic of the quantized Hall resistance and are crucial for estimating the charge carrier concentration.

The identification of these plateaus forms the basis for estimating the charge carrier concentration. By correlating the quantized Hall resistance values with the known current passing through the sample, the density of charge carriers involved in the QHE is inferred.

Subsequently, the values derived from the measurements are utilized to calculate the fine structure constant. This dimensionless constant is pivotal in the field of quantum electrodynamics, and its experimental determination validates the precision of quantum theory.

Finally, the obtained values are compared with those from existing literature. This comparison serves as a benchmark for the accuracy and reliability of the experimental approach and methods applied. It also provides a potential avenue for enriching the scientific corpus, either by corroborating established values or suggesting modifications based on the empirical findings.

3.1 Longitudinal Voltage Extrema Analysis

Within this section, a comparative analysis is executed across three distinct datasets, each characterized by variations in applied current and sample temperatures. This examination enables the correlation between these experimental conditions and their influence on the observed QHE.

For the dataset with an applied current of $100\mu A$ at a temperature of 3.5 K, the following extrema, depicted in Figure 3.1 have been cataloged:

- An extremum group centered around $B = 1.80$ T, with the voltage averaged over the interval $[1.80, 1.80]$ T being 0.09 V.
- An extremum group centered around $B = 2.34$ T, with the voltage averaged over the interval $[2.30, 2.36]$ T being 0.05 V.
- An extremum group centered around $B = 3.52$ T, with the voltage averaged over the interval $[3.49, 3.54]$ T being 0.20 V.
- An extremum group centered around $B = 4.62$ T, with the voltage averaged over the interval $[4.29, 4.94]$ T registering as negligible.
- An extremum group centered around $B = 5.98$ T, with the voltage averaged over $[5.98, 5.98]$ T being 0.29 V.

In the scenario of an applied current of $40\mu A$ at the same temperature of 3.5 K, the identified extrema, illustrated in Figure 3.2 are as follows:

- An extremum group centered around $B = 1.78$ T, with the voltage averaged over $[1.78, 1.78]$ T being 0.04 V.
- An extremum group centered around $B = 2.32$ T, with the voltage averaged over $[2.26, 2.39]$ T being 0.01 V.
- An extremum group centered around $B = 3.29$ T, with the voltage averaged over $[3.23, 3.35]$ T being 0.09 V.
- An extremum group centered around $B = 4.65$ T, with the voltage averaged over $[4.05, 5.24]$ T registering as negligible.

For the third dataset at an elevated temperature of 4.4 K with an applied current of $40\mu A$, the observed extrema, depicted in Figure 3.3 include:

- An extremum group centered around $B = 1.76$ T, with the voltage averaged over $[1.76, 1.76]$ T being 0.04 V.
- An extremum group centered around $B = 2.26$ T, with the voltage averaged over $[2.20, 2.32]$ T being 0.01 V.
- An extremum group centered around $B = 3.25$ T, with the voltage averaged over $[3.18, 3.33]$ T being 0.09 V.
- An extremum group centered around $B = 4.49$ T, with the voltage averaged over $[3.98, 5.00]$ T registering as negligible.
- An extremum group centered around $B = 5.90$ T, with the voltage averaged over $[5.90, 5.90]$ T being 0.13 V.

The analysis delineates the sensitivity of QHE manifestations to both the applied current and the operational temperature of the sample. Each dataset reveals unique voltage behavior at critical magnetic field strengths, reflecting the distinct conditions under which the sample was examined. These patterns provide a foundation for in-depth exploration of Hall voltages, identification of plateaus, and quantification of charge carrier concentration, thereby advancing towards the ultimate objective of calculating the fine structure constant.

The succeeding subsections will build upon these findings, incorporating the variability introduced by the different experimental setups to refine the understanding of the QHE and the sample's electronic properties.

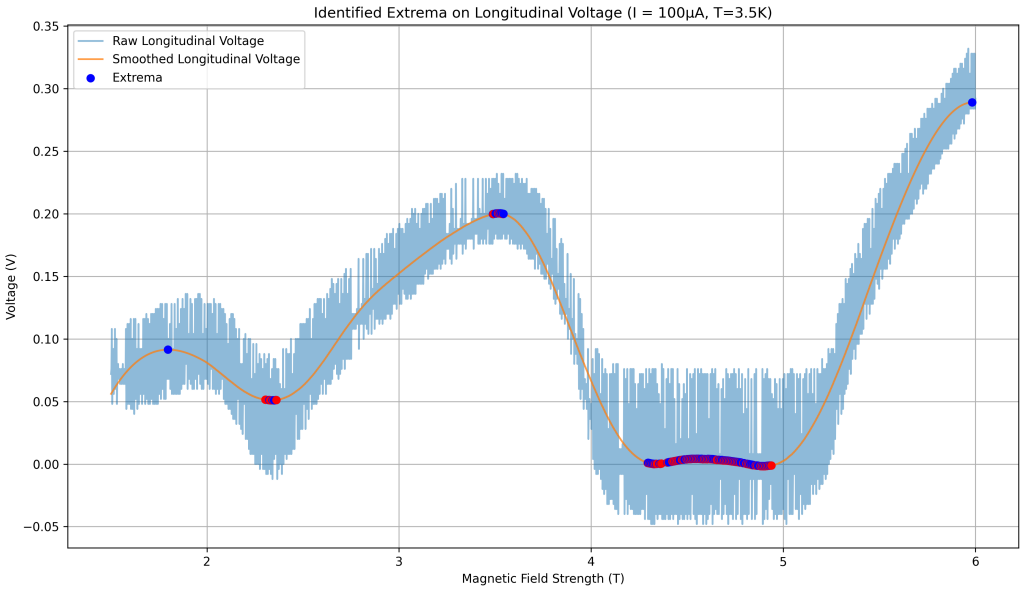

Figure 3.1: Extrema of longitudinal voltage where I=100µA and T=3.5K

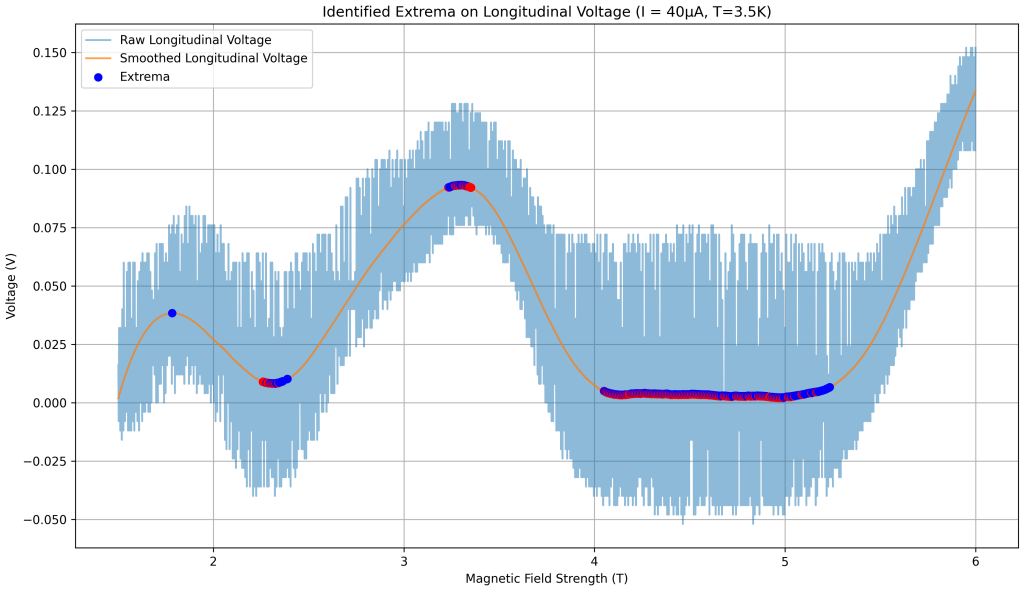

Figure 3.2: Extrema of longitudinal voltage where I=40µA and T=3.5K

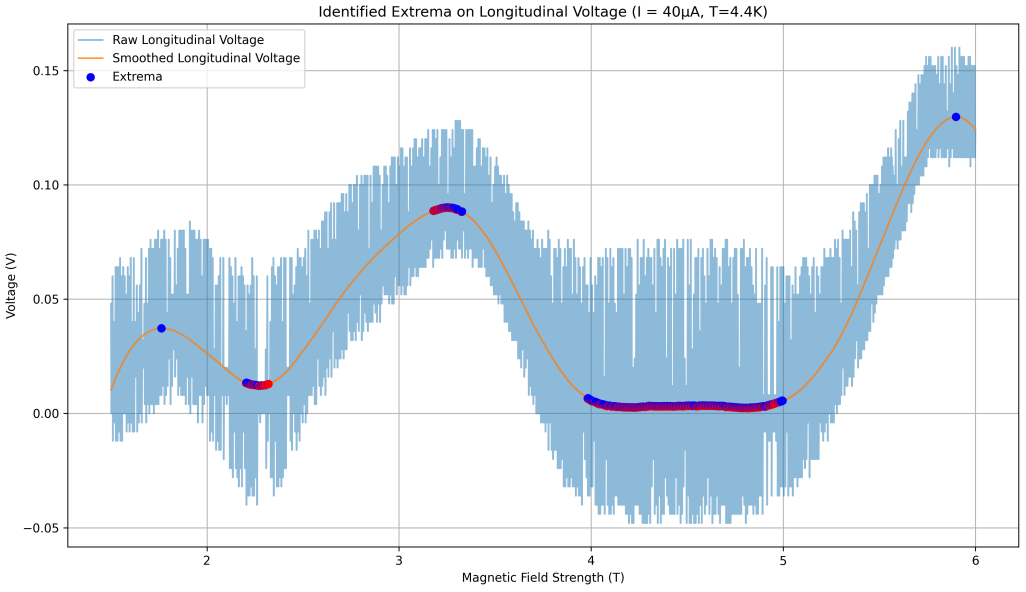

Figure 3.3: Extrema of longitudinal voltage where I=40µA and T=4.4K

3.2 Identifying the Hall Voltages and the Hall Plateaus

The QHE was investigated through the measurement of Hall voltages over specific intervals of magnetic field strengths, and the identification of Hall plateaus was conducted. For the experiment, configurations were set with variations in current and temperature.

In the configuration with a current of 100µA at 3.5K, the calculated average Hall voltages for the identified plateaus were as follows: 0.66V for the magnetic field interval of 2.28T to 2.4T, and 1.31V for the interval of 4.29T to 4.94T. These plateau regions are illustrated in Figure 3.4 , where the averaged Hall voltages are marked and presented alongside the raw transverse voltage data and its smoothed counterpart.

For a reduced current of 40µA at 3.5K, the average Hall voltages were found to be 0.26V in the magnetic field range of 2.25T to 2.4T, and 0.52V in the range of 4.05T to 5.24T. The corresponding plateaus for this configuration are depicted in Figure 3.5.

Upon increasing the temperature to 4.4K while maintaining the current at 40µA, the plateau average Hall voltages were obtained as 0.26V for the magnetic field interval from 2.2T to 2.35T, and 0.52V for the interval of 3.96T to 5.0T. The plateaus for this set of conditions are demonstrated in Figure 3.6.

The plotted data effectively showcase the presence of Hall voltage plateaus, as anticipated by the theory of the QHE. The consistency of voltage values across different currents and temperatures within the specific intervals reinforces the quantized nature of the Hall voltage, indicative of the established QHE.

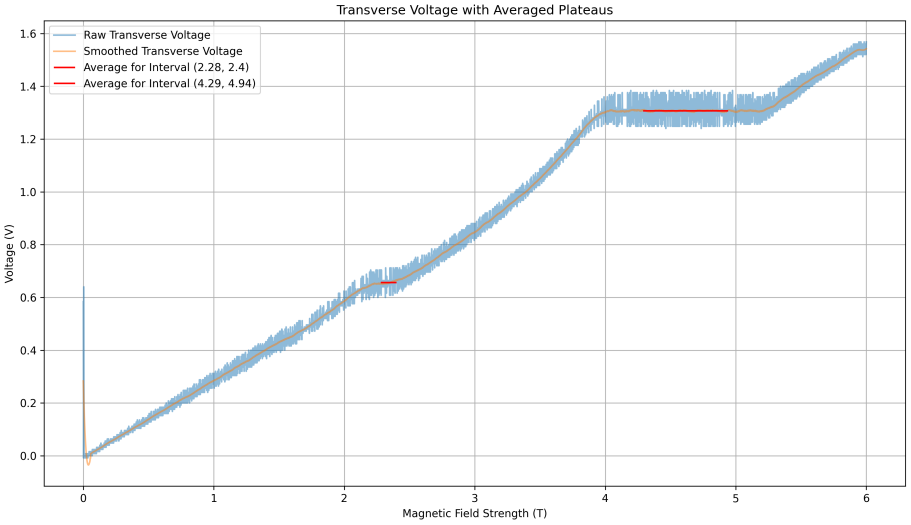

Figure 3.4: Identified Hall Plateaus at I=100µA and T=3.5K

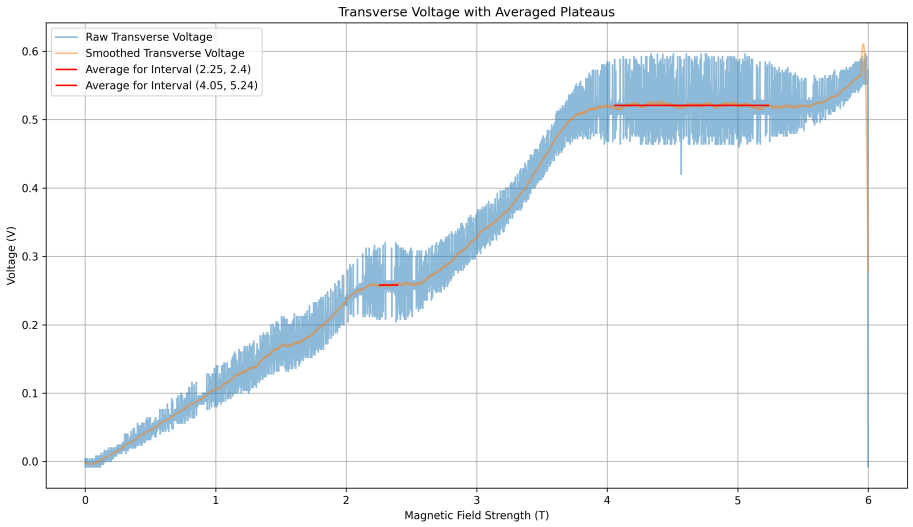

Figure 3.5: Identified Hall Plateaus at I=40µA and T=3.5K

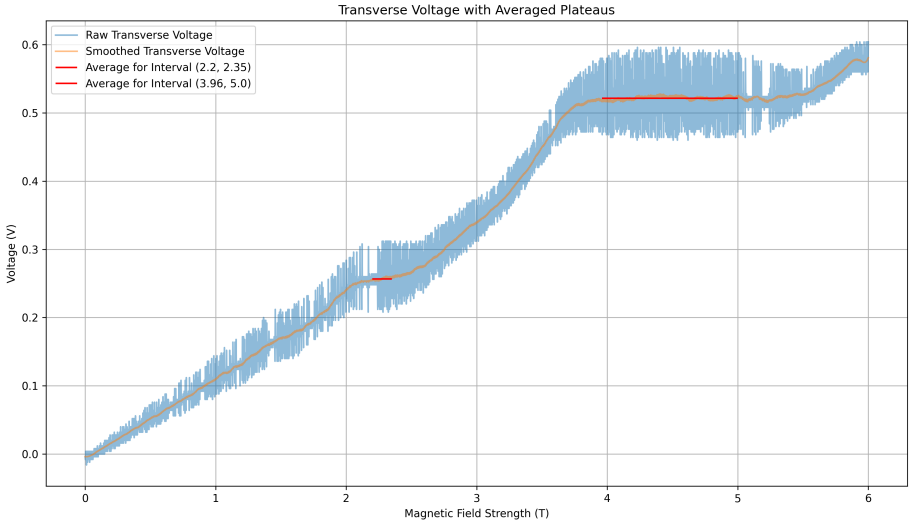

Figure 3.6: Identified Hall Plateaus at I=40µA and T=4.4K

3.3 Determination of Charge Carrier Concentration

The concentration of charge carriers in the sample was determined by utilizing the measured Hall voltages and the known current applied during the experiment. For a two-dimensional electron gas (2DEG), the Hall coefficient R_H is given by the ratio of the Hall voltage V_H to the current I_x, which is further related to the magnetic field strength B_z and the areal charge carrier concentration n per square meter, as described by the equation:

$$R_H = \frac{V_H}{I_x} = \frac{B_z}{n \cdot e} \tag{3.1}$$

This relationship enables the determination of the areal charge carrier concentration n using the known values of the magnetic field strength B_z, the Hall voltage V_H, and the elementary charge e.

Rearranging for charge carrier concentration yields:

$$n = \frac{B_z}{R_H \cdot e} \tag{3.2}$$

Where B_z represents the magnetic field strength at the plateau, V_H is the averaged Hall voltage at the plateau, and I_x is the current through the sample. Given the constant e (the elementary charge), the concentration n was calculated.

Substituting the respective values into the equation for each configuration, the concentration of charge carriers was ascertained. The detailed calculations and results are presented in Table 3.1, which includes the average Hall voltage for each plateau, the corresponding magnetic field strength, and the calculated charge carrier concentration.

Configuration	B_z **(T)**	V_H **(V)**	I_x **(A)**	R_H **(Ohm)**	n **(m^{-2})**
100µA 3.5K	4.5	1.31	1.00×10^{-4}	13100	2.14×10^{15}
40µA 3.5K	4.5	0.52	4.00×10^{-5}	13000	2.16×10^{15}
40µA 4.4K	4.5	0.52	4.00×10^{-5}	13000	2.16×10^{15}
100µA 3.5K	2.3	0.66	1.00×10^{-4}	6600	2.17×10^{15}
40µA 3.5K	2.3	0.26	4.00×10^{-5}	6500	2.21×10^{15}
40µA 4.4K	2.3	0.26	4.00×10^{-5}	6500	2.21×10^{15}

Table 3.1: Calculated charge carrier concentration for different configurations.

3.4 Determining the Fine Structure Constant

Given the resistance values R_H from the QHE measurements, the fine structure constant α can be calculated using the relationship:

$$\alpha = \frac{e^2}{h} \cdot \frac{1}{2\epsilon_0 \cdot c} = \frac{1}{R_H \cdot \nu} \cdot \frac{1}{2\epsilon_0 \cdot c} \tag{3.3}$$

Substituting the known values of e, ϵ_0, and c into the equations will yield the values of α for each configuration.

For the given resistances, the calculations are as follows:

For $R_H = 6600\ \Omega$ and $\nu = 4$:

$$\alpha_{100\mu A} = \frac{1}{2\epsilon_0 \cdot c} \cdot \frac{1}{R_H \cdot \nu} = \frac{1}{2\epsilon_0 \cdot c} \cdot \frac{1}{6600\Omega \cdot 4} \approx 7.14 \times 10^{-3} \tag{3.4}$$

For $R_H = 13100\ \Omega$ and $\nu = 2$:

$$\alpha_{40\mu A} = \frac{1}{2\epsilon_0 \cdot c} \cdot \frac{1}{R_H \cdot \nu} = \frac{1}{2\epsilon_0 \cdot c} \cdot \frac{1}{13100\Omega \cdot 2} \approx 7.19 \times 10^{-3} \tag{3.5}$$

Conclusion

The experimental values for the fine structure constant, α, were determined from the quantum Hall effect measurements for different configurations. For a Hall resistance of 6600 Ω with a filling factor $\nu = 4$, the calculated value of α was found to be approximately 7.14×10^{-3}. Similarly, for a Hall resistance of 13100 Ω and a filling factor $\nu = 2$, α was calculated to be approximately 7.19×10^{-3}. These values exhibit a deviation of approximately 1.5 percent from the accepted literature value of 1/137 or 7.29×10^{-3}, indicating a commendable level of accuracy in the experimental measurements given the complex nature of the quantum Hall effect.

The observed discrepancies could be attributed to several factors. Systematic limitations within the experimental setup, such as the precision of the resistance measurement or the stability of the magnetic field, may contribute to the variance. Additionally, the inherent fluctuating nature of the quantum Hall effect data, which can be affected by sample impurities, temperature variations, or electronic noise, may also play a role. These results underscore the challenges in high-precision measurements and highlight the importance of accounting for potential experimental limitations when interpreting quantum Hall effect data.

Bibliography

[1] given Literature

[2] Nave, R.: Hall Effect
Available online at: `http://hyperphysics.phy-astr.gsu.edu/hbase/magnetic/Hall.html`, last accessed on 01.11.2023